22nd International Conference on Renewable Energies and Power Quality (ICREPQ'24)
Bilbao (Spain), 26th to 28th June 2024

ISBN: 978-84-09-60656-6

Efficiency Analysis of an Interleaved Converter as Power Interface between a PEM Electrolyzer and a Photovoltaic Source.

Gianpaolo Vitale[1]

[1] ICAR, Institute for high performance computing and networking, National Research Council (CNR),
Via Ugo La Malfa, 153, 90146 Palermo. ORCID:0000-0002-5439-6835

Abstract. This paper deals with the conversion efficiency of an interleaved six-legs DC/DC converter used as an interface between a photovoltaic source and an electrolyzer. Different configurations of the photovoltaic sources are analysed, varying the numbers of the operated legs of the converters. The efficiency is affected by the high current required by the electrolyzer; however, the analysis shows that the optimal configuration of the PV source and of the number of the converter's operated legs can improve performance.

Key words. photovoltaic source; DC/DC converter; interleaved converter, PEM electrolyzer; efficiency; Hydrogen.

1. Introduction

Hydrogen can contribute to decarbonisation in electricity production, transportation, and industry; it is widely recognized as a clean energy carrier [1]. Hydrogen can be produced by water electrolysis; the supply power ranges from small systems (small-scale distributed production systems with power around 1kW or smaller) to large plants (as in central production facilities where power reaches MW) [2]. Three main electrolyzers (EL) adopting different technologies exist: alkaline, proton exchange membrane (PEM), and solid oxide (SO) [3]. Among them, Alkaline and PEM electrolyzers are available on the market.

Hydrogen's intrinsic "green" feature requires clean energy to be preserved. For this reason, renewable energy sources (RES) (e.g., wind turbines, photovoltaic) are the most appropriate for green hydrogen production [4,5]. Using RES for hydrogen production can improve the interconversion of electricity and Hydrogen and expand the hydrogen application [6]. The local production of Hydrogen can reduce countries' dependence on external energy suppliers [7]. Low power plants are gaining attention for using Hydrogen with natural gas as an energy source in residential contexts, as in the Capelle la Grande district of the Dunkerque Urban Community, where an experimental test allowed a reduction of carbon emissions of about 7% [8].

This paper deals with low-power PEM electrolyzers since they can be exploited to produce hydrogen for domestic applications and improve performance with a cheap system; it could help push the market toward green hydrogen production. The PEM electrolyzers show several advantages, such as a high current density (above 2A/cm^2), a low operational cost, and low ohmic drops due to the thinner electrolyte than the alkaline EL. The PEM EL shows fast response of the proton transport across the membrane. Hence, it can operate with a wide range of power inputs when it is supplied by RES [9].

The interfacing between the electrolyzer and the source is usually performed by a power converter tracking the maximum power point (MPP) and the matching between the input and output voltage [10,11,12]. The presence of a DC/DC converter offers many additional advantages, such as flexibility in PV source configuration and suitable dynamic control when abrupt variations of solar radiation occur [11,12]. Among the disadvantages there is the output ripple that can deteriorate the PEM membrane [13,14], and its efficiency that lowers the available power [4].

This paper analyses the efficiency of the interfacing converter employed between a photovoltaic (PV) source and a PEM electrolyzer. The analysis is performed by varying the PV configuration to highlight the role of the constraints imposed by the electrolyzer, the PV configuration, and the converter components.

2. PV source model

This paper adopts the one-diode four parameters model; the circuit is drawn in Figure 1. This model is obtained by the double diode model described in [15]. The characteristic equation is represented by (1).

$$\begin{cases} I = I_0 - e^{\{(V+IR_s)K_1+K_2\}} \\ I_0 = I_{ph} \\ K_1 = \dfrac{q}{AKT} \\ e^{K_2} = I_s \end{cases} \quad (1)$$

Where I and V represents the current and voltage at the cell's terminals, respectively; I_{ph} is the photogenerated current, R_s is the series equivalent resistance. The two parameters K_1 and K_2 define the cell behaviour based on the electron charge q, Boltzmann constant K, and temperature T, [K]. The single-diode model is based on the Shockley diode equation; it encompasses a diode quality factor A to consider both diffusion and recombination in the space charge layer. The series resistance R_s models the power losses due to the current circulating through different cell parts. The photo-generated current subtracted from the quantity flowing through the diode current gives the output current. A more complicated model can encompass a shunt resistance R_{sh} parallel connected to the diode; it reproduces power losses, usually resulting from manufacturing defects. An estimation for the value of the shunt resistance of a solar cell can be derived from the slope of the IV curve near the point of the short circuit current. Typical values for area-normalized shunt resistance are about 1kΩ·cm^2 for commercial solar cells.

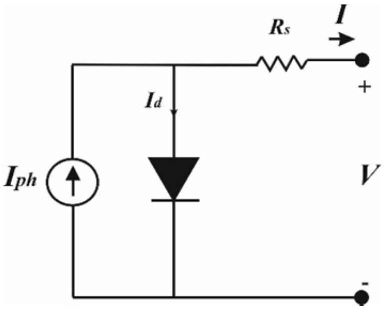

Figure 1. Equivalent circuit of a PV cell.

The four parameters K_1, K_2, Rs and I_0, are calculated by the short-circuit current (I_{sc}), the open circuit voltage (V_{oc}) and the voltage and current on the maximum power point (V_{mp} and I_{mp}) by the equations (2):

$$\begin{cases} K_1 = \dfrac{\dfrac{I_{mpp}}{I_0 - I_{mpp}} + log\left[1 - \dfrac{I_{mpp}}{I_0}\right]}{2\,V_{mpp} - V_{oc}} \\ R_s = \dfrac{V_{mpp} - \dfrac{I_{mpp}}{(I_0 - I_{mpp})K_1}}{I_{mpp}} \\ K_2 = log[I_0] - V_{oc}\,K_1 \\ I_0 = I_{sc} + e^{\{(I_{sc}\,R_s)K_1 + K_2\}} \end{cases} \tag{2}$$

The non-linear system (2) is solved by a recursive form:

1. It is assigned I_0=I_{sc};
2. I_0 is substituted in the first equation in (2) and K_1 is obtained.
3. I_0 and K_1 are substituted in the second and in the third equations in (2), giving R_s and K_2.
4. Finally, K_1, K_2, and R_s are substituted in the fourth equation in (2), retrieving and a new value of I_0.

The convergence is reached in few steps. The values of the model parameters versus solar irradiance, G, and temperature, T, are calculated by the open circuit voltage V_{oc} and the short circuit current I_{sc}, based on the values given by the manufacturer in standard conditions (1000W/m^2, T=25 °C), $V_{oc(stc)}$ and $I_{sc(stc)}$. The manufacturer gives the thermal coefficient Δ to evaluate the V_{oc} variation.

$$V_{oc} = V_{oc(stc)} + \Delta(T - T_{stc}) \tag{3}$$

$$I_{sc} = \frac{G}{G_{stc}} I_{sc(stc)} \tag{4}$$

The adopted model does not consider the shunt resistance R_{sh}, since, with Si-crystalline cells, it has a high value. Therefore it has relatively little effect on the general module behavior (low shunt current loss).

In the paper, the PV cells are connected in series to form an array; the corresponding parameters can identify the equivalent circuit model. The array is designed based on the desired voltage at the maximum power; more arrays are connected in parallel to increase the current.

The photovoltaic cell for supplying the PEM electrolyzer is a Polycrystalline Silicon Cell delivered by Risen Solar Technology [16]. It is a 156 x 156 mm cell with a thickness of 200µm (wafer). The main electrical characteristics are summarized in Table 1.

Table 1. Characteristic parameters of the solar cell (measured under STC standard test conditions 1000W/m2, AM 1.5, 25 °C).

Parameter	value	unit
Pmpp	4.33	W
Vmpp	0.53	V
Impp	8.17	A
Voc	0.635	V
Isc	8.693	A
FF	78.44	%

Table 2. Parameters of a single cell

Parameter	value
K_1 [V^{-1}]	36.92
K_2	-18.4
Rs [Ω]	0.0035
R_{sh} [Ω]	5.87

3. PEM electrolyzer operating principle and equivalent model

Hydrogen can be produced by three different solutions: alkaline, SO, and PEM (Proton Exchange Membrane). PEM electrolysis cells adopt a solid polymer electrolyte concept; they offer, among several advantages, high current density (above 2A/cm^2), low operational cost, and reduced ohmic drops since the electrolyte is thinner than the alkaline EL. The proposed analysis is focused on a PEM Electrolizer (EL). Moreover, the PEM EL shows a fast response of the proton transport across the membrane; consequently, it can operate with a wide range of input power. This feature is of interest when renewable energy sources deliver the power. The chemical reaction to obtain hydrogen is described by eq. (6) in which the Gibbs energy (237 kJ.mol^{-1}) and the lost energy (48.6 kJ.mol^{-1}) are considered:

$$H_2O + 237.2\left[\frac{kJ}{mol_{(Gibbs)}}\right] + 48.6\left[\frac{kJ}{mol_{(heat)}}\right] \rightarrow H_2 + \frac{1}{2}O_2 \quad (5)$$

The PEM EL operation is shown in Figure 2. The water molecule is divided into oxygen and protons and electrons are obtained according to the sub-reaction:

$$H_2O \rightarrow 2H^+ + \frac{1}{2}O_2 + 2e^- \quad (6)$$

The electrons flow outside the anode, forming a current (flowing through the anode), whereas the protons flow through the membrane. The protons are combined with electrons in the cathode, and hydrogen is obtained:

$$2H^+ + 2e^- \rightarrow H_2 \quad (7)$$

The adopted electrolyzer is a PEM system delivered by HELIOCENTRIS® Company, type NMH2 1000. It is also available for educational purposes [17]. For this work, only the stack of the PEM electrolyzer is considered without the converter given by the manufacturer. The electrolyzer is supplied by the Photovoltaic source by an interleaved converter to discuss its efficiency varying the source configuration. The electrolyzer has a very thin membrane (around 25 μm) to minimize ohmic losses. The specifications are summarized in Table 2.

Table 3. Characteristic parameters of the NMH2 1000 PEM electrolyzer by HELIOCENTRIS®.

Parameter	Value	Unit
Rated electric power	400	W
Stack voltage operating range	4.2 - 8	V
Stack current range	0 - 50	A
Operating temperature range	288.15 – 313.15	K
Hydrogen outlet pressure	10.5	bar
Cells number	3	-
Active area section	50	cm^2
Hydrogen flow rate at STP (Standard Temperature and Pressure: 20°C, 1 bar)	0 - 1	SLPM (Standard l/min)

The electrolyzer has been modelled by a circuit derived from the electrical parameters. The stack starts operating at 4.2V; increasing the voltage, the current rises linearly up to the rated value that corresponds to 8V, 50A. The equivalent series resistance R_{int_eq} is calculated by:

$$R_{int\_eq} = \frac{V_{rated} - V_{int}}{I_{rated}} = 0.076\ \Omega \quad (8)$$

where V_{rated} and I_{rated} are the voltage and current applied to the electrolizer at the maximum power, V_{int} is the internal voltage of the electrolyzer. The equivalent static circuital model shown in Figure 2; the hydrogen is produced by the current flowing through V_{int}, whereas the current flowing through R_{int_eq} causes losses.

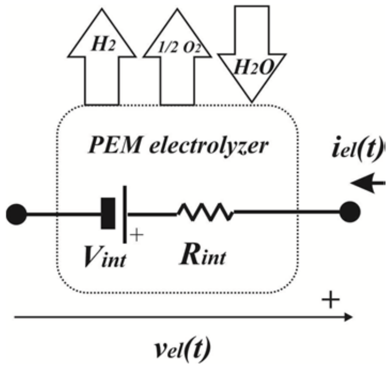

Figure 2. Circuital model of the electrolyzer.

4. The interleaved converter under study

The interfacing DC/DC converter allows tracking the optimal matching between the source and the load, varying the solar radiation; hence, the operating points are those calculated in correspondence with the maximum power versus voltage curves defined by the PV source. Unfortunately, the converter is subjected to losses mainly due to switching power devices and Joule conduction losses. Losses have an impact on converter efficiency; this is discussed in this paper for different PV configurations.

An interleaved boost converter was used to obtain good efficiency. This converter shares the current among several inductors and power switches, minimizing the joule losses. It increases the efficiency since Joule losses increase with the square of the current; in addition, it guarantees a low output current ripple [17]. The converter shows a six-leg structure and has already been proposed and analysed for automotive applications [18,19]. The efficiency is calculated in operating conditions and with real components, considering the curves obtained with a single-leg operation, two legs, and so on up to six legs. In this way, the best number of operated legs can be selected for given output current. The electric scheme is drawn in Figure 3. The list of commercial devices employed for this converter, including parasitic components, is given in Table 3.

Differently from the automotive application described in [19,20], where the output voltage is maintained constant, varying the input, here the power available from the PV source imposes the current to the electrolyzer; it is obtained by a suitable output voltage given by the converter.

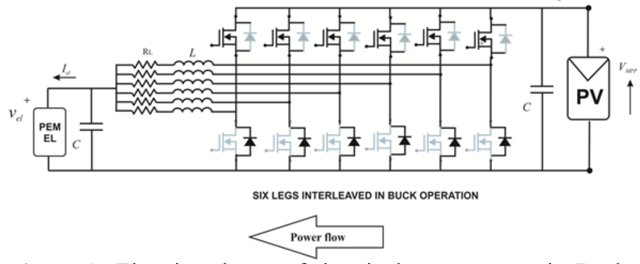

Figure 3. Electric scheme of the six legs converter in Buck operation

Table 3. Commercial components of the six legs interleaved converter.

Symbol	Rated value	Supplier	Code
L	I_L = 10 A, L = 500 uH, R_L = 50 mΩ	Vishay	IHV15BZ500
C	560 µF, Resr = 160 mΩ	Epcos	B43511A 4567M007
MOSFET	V_{DSS} = 650 V, R_{DS}(on) = 110 mΩ@25 °C; I_{DS} = 25 A	Infineon Techn.	IPA60R125CP CoolMOS

The power balancing between the PV source and the load (neglecting the converter losses) can be expressed by:

$$V_{mp} \cdot I_{mp} = I_{el}^2 \cdot R_{int} + I_{el} \cdot V_{int} \tag{9}$$

The current supplied to the electrolyzer depends on the voltage at its terminals, subtracted by the internal voltage, and divided by its internal resistance as in (10):

$$I_{el} = \frac{V_{el} - V_{int}}{R_{int}} \tag{10}$$

By substituting eq. (10) in (9), a second-order equation is obtained; the positive solution gives the output voltage of the converter to be applied to the electrolyzer for obtaining the best matching condition.

$$V_{el}^2 - V_{el} \cdot V_{int} - P_{mp} \cdot R_{int} = 0 \tag{11}$$

The converter efficiency is calculated based on the losses, and it is obtained as a function of the input current. The losses are given by switching and conduction losses in MOSFETs, conduction and recovery losses in the diodes, joule and magnetic losses in inductors, and Joule losses in the output capacitance.
The switching losses for a MOSFET device are:

$$P_{SW} = \frac{1}{2} V I (t_{on} + t_{off}) f_s \tag{12}$$

where V is the MOSFET voltage between drain and source in blocking state, I is the conduction current during conduction, f_s is the switching frequency, t_{on} and t_{off} are the turn-on and turn-off time of the device, respectively. For the selected MOSFET $t_{on}=t_{off}$=5ns.

The conduction losses on one MOSFET are:

$$P_c = D\left[R_{ds(ON)}\left(\bar{I}_L^{\,2} + \frac{\Delta I_L^2}{12}\right)\right] \tag{13}$$

where D is the duty cycle of the converter, $R_{ds(ON)}$ is the conduction resistance of the MOSFET; the root mean square of the current is calculated as the sum of the maximum average value summed to the AC periodic (ΔI_L) part which is a triangular waveform.

The power loss on the diode is given by both the conduction and the recovery losses; the conduction losses are:

$$P_{D\_cond} = (1 - D)\left[V_\gamma \bar{I}_D + R_D\left(\bar{I}_D^{\,2} + \frac{\Delta I_L^2}{12}\right)\right] \tag{14}$$

where V_γ is the forward drop voltage of the diode and R_D its conduction resistance. The reverse recovery losses of the diode are calculated by its reverse recovery current (I_{rr}) and reverse recovery time (t_{rr}); V is the voltage applied to the diode in reverse bias.

$$P_{D\_rr} = \frac{1}{2} V t_{rr} I_{rr} f_s \tag{15}$$

In our case, t_{rr} = 430 ns, I_{rr} = 42 A for the diode that is integrated into the MOSFET.

The power loss on one inductor is calculated by the square of the rms value of the current multiplied for its parasitic resistance R_L:

$$P_L = R_L\left(\bar{I}_D^{\,2} + \frac{\Delta I_L^2}{12}\right) \tag{16}$$

The magnetic losses are calculated based on the Revised Generalized Steinmetz Equation (RGSE) following the methods explained in [19].

The power loss on output capacitor, whose parasitic resistance is R_{ESR}, in the worst case is given by:

$$P_{C\_C} = R_{ESR}(1 - D)\left(\frac{\Delta I_L}{2\sqrt{3}}\right)^2 \tag{17}$$

Finally, the converter efficiency is calculated as:

$$\eta_{\_n}(I_{mp}) = \frac{P_{mp}}{P_{mp} + P_{total\_losses}} \tag{18}$$

Where $\eta_{\_n}(I_{mp})$ is the efficiency with n legs operated, calculated versus the input current, the calculation is performed for n= {1, 2,…,6}.

5. Results

The converter's efficiency is evaluated for four configurations of the photovoltaic source. The overall power of the source is fixed; it is imposed by the load. The connection of the arrays allows for different supply voltage of the converter. The different input voltage imposes a different duty cycle on the converter, affecting losses. The converter efficiency is calculated for each configuration, considering the legs operated for n= {1, 2,…,6}.

The basic PV array is composed of a series connection of 16 cells, obtaining a voltage of about 8.5 V at the maximum power point. The four configurations are obtained based on different connections of eight arrays.

A. Eight arrays parallel connected

The first considered configuration comprises eight parallel array connected as schematically shown in Figure 4. Since each array can deliver about 8.17A at the maximum power point, the theoretical available power is about 550W; however, it is reduced by the efficiency of the DC/DC converter before supplying the electrolyzer, whose rated power is 400W.

The current versus voltage and the power versus voltage curves of the PV source are drawn in Figures 5 and 6, respectively, together with the load curve. It can be noted that, without using the interface converter. the optimal matching would be achieved only in one point (approximatively corresponding to 700 W/m^2). Hence, the DC/DC converter is adopted to retrieve the optimal matching for whatever solar radiation.

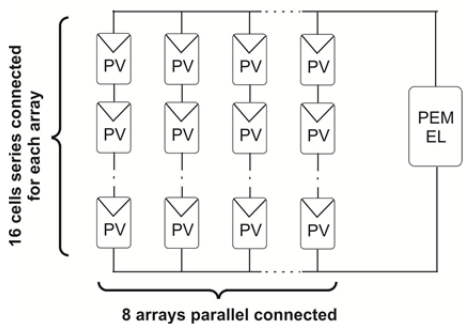

Figure 4. PV configuration with eight arrays parallel connected.

The efficiency curve of the DC/DC converter is calculated by eq. (18) in this configuration, and it is drawn in Figure 7. It can be noted that the best efficiency is retrieved by six legs operated; it shows a maximum equal to about 0.9 for 100W of input power, and then it decreases. The fewer branches are in operation, the lower the efficiency.

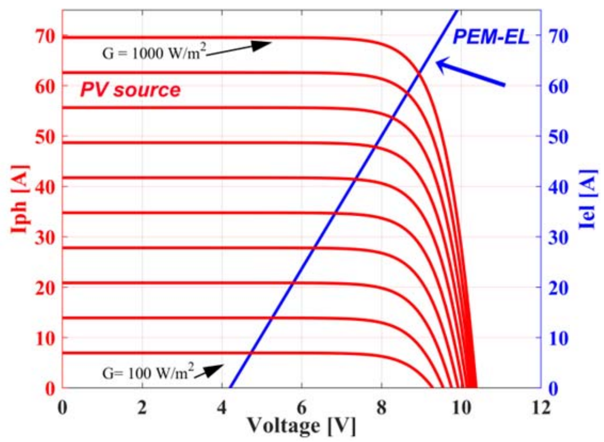

Figure 5. Current versus voltage curves of the PV configuration with eight arrays parallel connected and load curve.

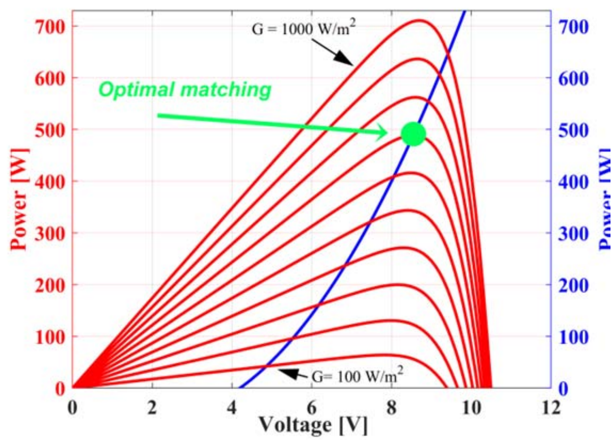

Figure 6. Power versus voltage curves of the PV configuration with eight arrays parallel connected and load curve.

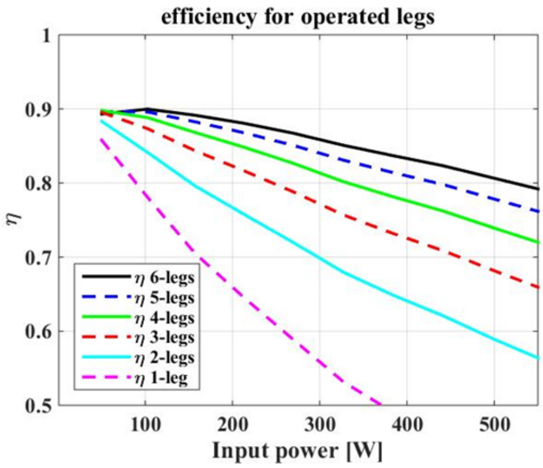

Figure 7. Efficiency calculated with eight parallel connected arrays.

B. Series connection of two sets of four arrays parallel connected.

By adopting two sets of four arrays, an overall increase in efficiency can be appreciated; from a power of 100W, the best number of operated legs corresponds to the maximum, i.e., six. A crossing point of the curves can be recognized; for input power lower than 100W, best values are given with a single-leg operation, as shown in Figure 8.

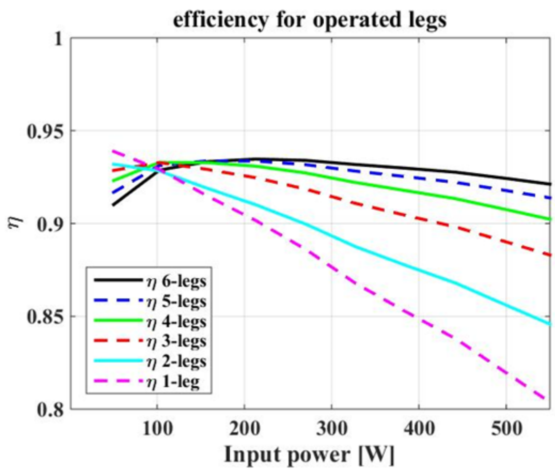

Figure 8. Efficiency calculated with a series connection of two sets of four arrays parallel connected.

C. Series connection of four sets of two arrays parallel connected.

By adopting four sets of two arrays, the crossing point of the efficiency curves is displaced towards about 250W, as shown in Figure 9; it means that, for lower power, it is convenient to have some legs on stand-by.

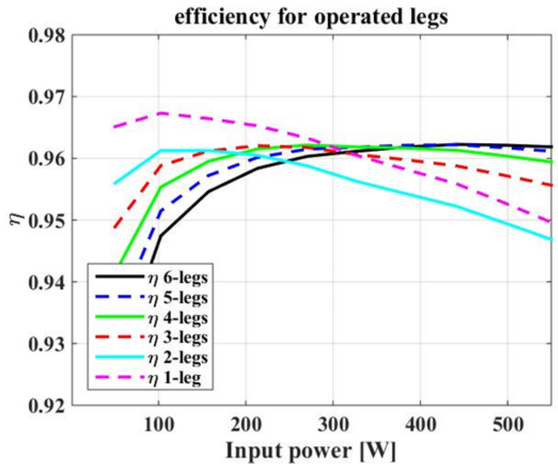

Figure 9. Efficiency calculated with a series connection of four sets of two arrays parallel connected.

D. Series connection of eight arrays

With eight arrays connected in series the best efficiency is achieved by only one leg operated as drawn in Figure 10.

This operation with a single leg, however, is calculated based on the inductor's parameters shown in Table 3. Consequently, the inductor and the MOSFET should be designed for higher currents. The actual efficiency will be lower, even if the comparison among legs remains realistic.

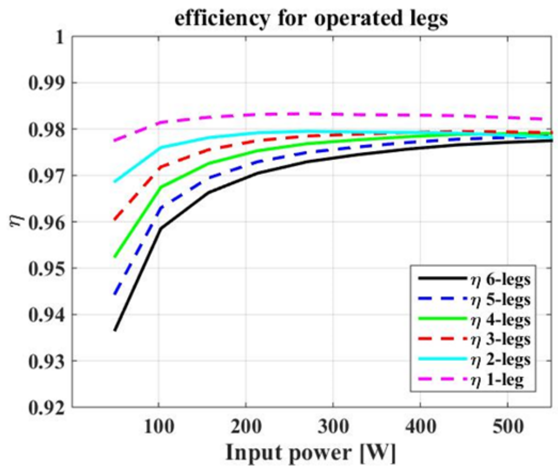

Figure 10. Efficiency calculated with eight arrays connected in series.

6. Sensitivity analysis

The sensitivity analysis aims to identify the main causes of the efficiency degradation. The parameters given by the manufacturer are subjected to variations due to the tolerances and temperature. Besides, additional parasitic resistances given by the electrical connections are always present; they add to the parasitic values of the components. Finally, all parameters vary with temperature also.

Three parameters have been considered: the voltage drop across the power diodes V_{Υ}, the conduction resistance of the MOSFETs R_{on}, and the parasitic resistance of the power inductor R_L. In the last section, results have been obtained with the values extracted by data-sheets, here the following values are adopted: V_{Υ} ={0.6V, 0.9V, 1.2V, 1.5V}; R_{on} = {0.1 Ω, 0.2 Ω, 0.3 Ω, 0.4 Ω,}; R_L = {0.1 Ω, 0.2 Ω, 0.3 Ω, 0.4 Ω,}. The efficiency is calculated for the two legs configuration since it gives the best performance with all arrays series connected. The related efficiency curves are drawn in Figures 11, 12, and 13.

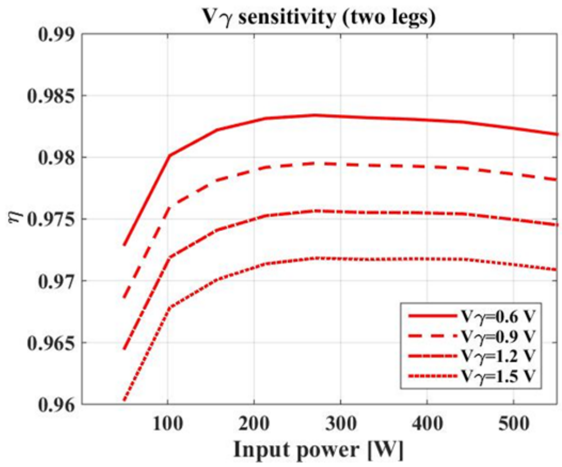

Figure 11. Efficiency calculated for different values of the diodes drop voltage

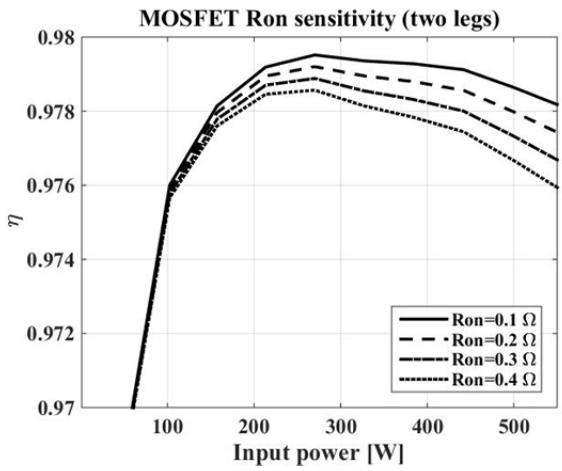

Figure 12. Efficiency calculated for different values of the MOSFET conduction resistance.

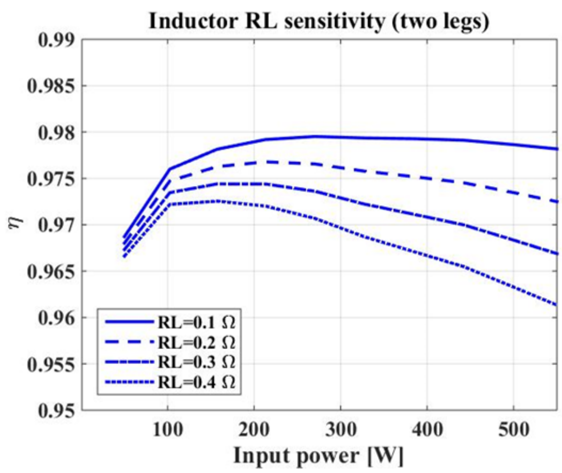

Figure 13. Efficiency calculated for different values of the Inductor parasitic resistance.

Table 4 summarizes the values obtained at rated power and the percent variations. The value indicated with * is the reference one adopted for calculation in the last section.

Table 4. Efficiency at rated power

Component	efficiency	%
Diode Vγ=0.6 V	0.9818	+0.38
Diode Vγ=0.9 V	0.9781*	-
Diode Vγ=1.2 V	0.9744	-0.38
Diode Vγ=1.5 V	0.9708	-0.75
MOSFET Ron=0.1Ω	0.9781*	-
MOSFET Ron=0.2Ω	0.9773	-0.08
MOSFET Ron=0.3Ω	0.9766	-0.15
MOSFET Ron=0.4Ω	0.9758	-0.24
Inductor R_L=0.1Ω	0.9781*	-
Inductor R_L=0.2Ω	0.9723	-0.59
Inductor R_L=0.3Ω	0.9666	-1.18
Inductor R_L=0.4Ω	0.9610	-1.75

7. Discussion

The different efficiency values obtained for each array configurations and operated legs result from the loss distribution within the converters' components. The switching losses play a marginal role due both to the low switching frequency (20kHz) and to the minimal rise and fall time of the adopted MOSFETs (5μs). Instead, conduction losses are relevant; concerning the power MOSFETs, they are quadratic with the current, proportional to R_{on}, and proportional to the duty cycle (*D*); with reference to the power diodes, they are linear with the current, proportional to the conduction drop voltage, and proportional to (*1-D*).

The different configurations allow a different input voltage; it implies a duty cycle of the converter (operated in step-down mode) that increases with the same input voltage. From Figure 11, it can be noted that eight arrays in series give higher voltages; consequently, a higher duty cycle is imposed on the MOSFETs (and a lower one on the power diodes). The diodes suffer from the drop voltage, greatly contributing to the efficiency degradation. Raising the input voltage, the higher duty cycle helps to lessen the losses due to the power diodes.

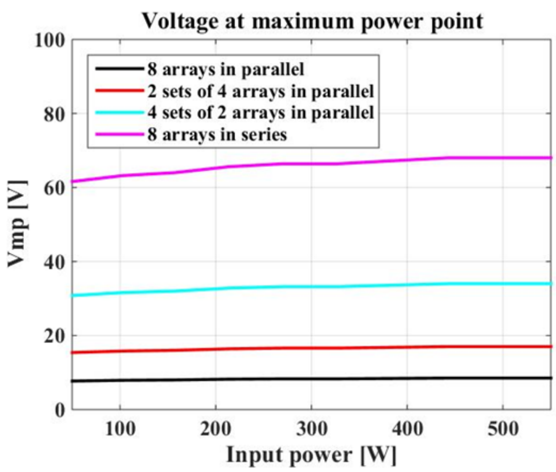

Figure 11. Voltage at the maximum power point versus power for different PV source configurations.

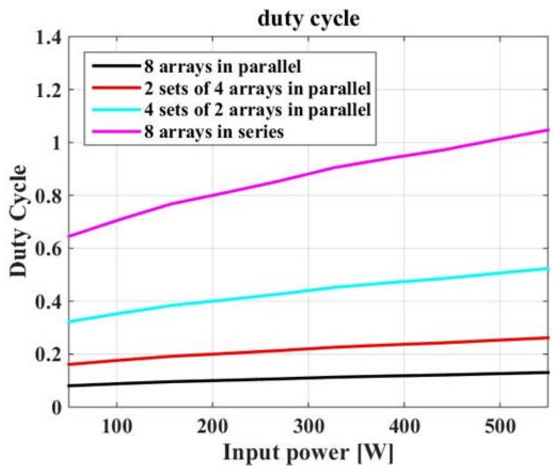

Figure 12. Duty cycle of the converter versus power for different PV source configurations.

The best efficiency is hence obtained by eight arrays connected in series; however, in operating conditions it is preferable to use at least two legs to minimize the ripple. Finally, the same configuration can be used only up to 500W of input power since the duty cycle would exceed the limit unitary value that is sufficient to supply the electrolyzer because of the excellent efficiency.

Concerning the sensitivity to the parasitic parameters, the greatest worsening is due to the equivalent parasitic resistance of the inductor; it is more evident increasing power. On the other hand, the MOSFET give a low contribution. The drop voltage of the diode gives a constant contribution varying the power.

8. Conclusions

The high current required by the electrolyzer affects the efficiency of the interfacing converter. Albeit the interleaved configuration allows sharing of the current among the operated legs, the different features of conduction loss distribution versus the current, quadratic and linear in powers MOSFETs and diodes, respectively, give different results in terms of efficiency depending on the input voltage range. In the MOSFETs the conduction losses benefit of a low conduction resistance and the switching losses can be minimized by a relatively low switching frequency and fast switching devices. The power diodes suffer of the drop voltage during conduction.

The best choice of the PV configuration corresponds to the higher input voltage given by the series connection of all arrays. It allows for reducing the number of required legs, making the converter cheaper; however, adopting at least a couple of operated legs allows minimizing the ripple and gives a valuable redundancy for fault tolerance robustness.

This analysis showed that the interfacing converter topology can be simplified with a suitable choice of the configuration of the photovoltaic source.

Future research directions can be summarized as follows: with reference to power components, it would be preferable to avoid power diodes by using MOSFETs in synchronous configuration since, albeit MOSFES losses are quadratic with current, the low value of the conduction resistance minimizes the dissipated power; the power inductors are always interested by current and their parasitic resistance must be minimized considering the layout design as well.

Acknowledgement

The author is grateful to Technician *Giampiero Rizzo* for the support in setting up the Hardware and software of the computational system to carry out the simulations given in this paper.

References

[1] Guilbert, D., Vitale, G. (2021). Hydrogen as a clean and sustainable energy vector for global transition from fossil-based to zero-carbon. Clean Technologies, 3(4), 881-909.
[2] Hydrogen Production: Electrolysis. Available online: https://www.energy.gov/eere/fuelcells/hydrogen-production-electrolysis (accessed on 25 feb 2024).
[3] Buttler, A.; Spliethoff, H. Current status of water electrolysis for energy storage, grid balancing and sector coupling via power-togas and power-to-liquids: A review. Renew. Sustain. Energy Rev. 2018, 82, 2440–2454.
[4] Abdelkareem, M. A., Abdelghafar, A. A., Mahmoud, M., Sayed, E. T., Mahmoud, M. S., Alami, A. H., ... & Olabi, A. G. (2023). Optimized solar photovoltaic-powered green hydrogen: Current status, recent advancements, and barriers. Solar Energy, 112072.
[5] Bilgen E. Solar hydrogen from photovoltaic-electrolyzer systems. Energy Convers Manage 2001;42(9):1047–57.
[6] Ahmad, G. E., & El Shenawy, E. T. (2006). Optimized photovoltaic system for hydrogen production. Renewable Energy, 31(7), 1043-1054.
[7] Yodwong, Burin, et al. "AC-DC converters for electrolyzer applications: State of the art and future challenges." Electronics 9.6 (2020): 912.
[8] The GRHYD demonstration project. Available online: https://www.engie.com/en/businesses/gas/hydrogen/power-to-gas/the-grhyd-demonstration-project (accessed on 25 Feb 2024).
[9] Guilbert, D.; Vitale G. Dynamic emulation of a PEM electrolyzer by time constant based exponential model. *Energies* 2019, 12(4), 750
[10] Yodwong B. ; et al. AC-DC converters for electrolyzer applications: State of the art and future challenges. Electronics 2020, 9.6 (2020): 912.
[11] Bilgen E. Solar hydrogen from photovoltaic-electrolyzer systems. Energy Convers Manage 2001, 42(9):1047–57.
[12] Ahmad G. E.; & El Shenawy E. T. Optimized photovoltaic system for hydrogen production. Renewable Energy 2006. 31(7), 1043-1054.
[13] Buitendach, H. P.; Gouws, R.; Martinson, C. A.; Minnaar, C.; Bessarabov, D. Effect of a ripple current on the efficiency of a PEM electrolyser. Results in Engineering 2021, 10, 100216.
[14] Parache, F. ; Schneider H. ; Turpin C. ; Richet N. ; Debellemanière O. ; Bru, É.; Marot C. Impact of power converter current ripple on the degradation of PEM electrolyzer performances. Membranes 2022, 12(2), 109.
[15] Di Piazza, M., Vitale, G. (2010). Photovoltaic field emulation including dynamic and partial shadow conditions. Applied Energy, 87(3), 814-823.
[16] https://www.enfsolar.com/pv/cell-datasheet/919 accessed on Jan, the 22th, 2024.
[17] https://www.heliocentrisacademia.com/hydrogen-generator/p1520?currency=usd accessed on Jan, the 22th, 2024.
[18] Kolar, J. W., Krismer, F., Lobsiger, Y., Muhlethaler, J., Nussbaumer, T., & Minibock, J. (2012, March). Extreme efficiency power electronics. In 2012 7th International Conference on Integrated Power Electronics Systems (CIPS) (pp. 1-22). IEEE.
[19] Pipitone, E., Vitale, G. (2020). A regenerative braking system for internal combustion engine vehicles using supercapacitors as energy storage elements-Part 1: System analysis and modelling. Journal of Power Sources, 448, 227368.
[20] Pipitone, E., Vitale, G. (2020). A six legs buck-boost interleaved converter for KERS application. Renewable Energy & Power Quality Journal, Volume No.18, June 2020. https://www.repqj.com/RE&PQJ-18-5.html.